Electronic states in quantum rings: electric field and eccentricity effects

2002 J. Phys.: Condens. Matter 14 259

(http://iopscience.iop.org/0953-8984/14/2/312)

INSTITUTE OF PHYSICS PUBLISHING JOURNAL OF PHYSICS: CONDENSED MATTER

J. Phys.: Condens. Matter **14** (2002) 259–270 PII: S0953-8984(02)28901-8

Electronic states in quantum rings: electric field and eccentricity effects

L A Lavenère-Wanderley[1], A Bruno-Alfonso[2] and A Latgé[1]

[1] Instituto de Física, Universidade Federal Fluminense, Avenida Litorânea sn, 24210-340, Niterói-RJ, Brazil
[2] Departamento de Matemática, Faculdade de Ciências, Universidade Estadual Paulista, Avenida Luis Edmundo Carrijo Coube sn, 17033-360, Bauru-SP, Brazil

E-mail: latge@if.uff.br

Received 13 September 2001, in final form 31 October 2001
Published 13 December 2001
Online at stacks.iop.org/JPhysCM/14/259

Abstract

The polarization effects of in-plane electric fields and eccentricity on electronic and optical properties of semiconductor quantum rings (QRs) are discussed within the effective-mass approximation. As eccentric rings may appropriately describe real (grown or fabricated) QRs, their energy spectrum is studied. The interplay between applied electric fields and eccentricity is analysed, and their polarization effects are found to compensate for appropriate values of eccentricity and field intensity. The importance of applied fields in tailoring the properties of different nanoscale materials and structures is stressed.

1. Introduction

The electronic energy spectrum and wavefunctions of nanostructures are quite sensitive to electric fields due essentially to the induced polarization of the spatial carrier distribution. This property may be used to control and modulate the intensity of photocurrents and light emission of optoelectronic devices. In particular, a remarkable decrease of the photoluminescence signal and a red shift in the photoluminescence peak position in GaAs–(Ga, Al)As quantum wells, for increasing electric field intensity, was reported two decades ago by Mendez *et al* [1]. Electric field effects on other heterostructures, such as quantum wires and dots, have also been investigated. For spherical quantum dots, a quasi-linear dependence on the electric field was predicted for the electroabsorption spectrum in the strong electric field regime [2]. The influence of axially applied electric fields on exciton binding energy, Stark shift and oscillator strength in quantum disks has been studied [3]. By changing the disk diameter and height, it was shown that the red Stark shift and the oscillator strength may be controlled. A general result is the appearance of new transitions which are forbidden when the electric field intensity is zero [4].

Among semiconductor low-dimensional systems, quantum rings (QRs) are of special interest, mainly due to their unique topology. The effective dimensionality of such structures may range from quantum-dot to quantum-well-wire regimes, depending on the geometrical sizes of the rings. The experimental realization of nanoscopic semiconductor QRs has been possible due to the large progress in the nanotechnology of self-assembled structures, such as those based on InGaAs [5, 6]. The occurrence of persistent currents (PCs) when QRs are threaded by magnetic fields is, perhaps, their most interesting property. Mailly *et al* [7] found PCs in semiconductor GaAs–(Ga,Al)As rings grown by molecular beam epitaxy techniques. The measured resistance signal showed Aharonov–Bohm oscillations, which are direct consequences of the ring topology. Also, Lin and Chui [8] reported PCs in toroidal carbon nanotubes, which may suffer metal–semiconductor transitions under variations of the threading magnetic flux. Recently, capacitance and transmission spectroscopy have been used to study self-organized InAs ring-like structures embedded in a GaAs matrix [9]. Interband absorption measurements were performed for neutral dots and rings, and the corresponding oscillator strengths show very different behaviours. The explanation for this is based on the interplay between Coulomb and quantization energies in such systems. A detailed study of the electronic states in the quantum limit is fundamental for the optical characterization of QRs [10]. While axially applied electric fields do not affect the axial symmetry of quantum disks [3], in-plane fields do, and may drastically change the corresponding electronic spectrum. In this respect, in-plane applied electric fields in QR structures were shown to break the wavefunction symmetry, to couple different angular momenta and to affect the interband oscillator strength [11]. Studies in those directions should lead to important technological applications, such as the fabrication of self-assembled QRs embedded in a field-effect transistor structure, where the number of electrons per ring may be controlled [6].

For the case of donor impurities in QRs with infinite barriers [12], the impurity binding energies are strongly affected by the ring hollow, since even for quite small internal radii the binding energy values for the corresponding QD limit are not attained. The sizes of the QRs are also shown to be fundamental in determining the electronic motion inside these low-dimensional structures. Axial magnetic fields distort the impurity states, and strongly modify the impurity density of states. Also, excitation-spectrum and oscillator-strength calculations of excitons in GaAs QRs pierced by magnetic fields have shown [13] that, for currently realizable QRs, excitons behave to a large extent as those in quantum dots of similar dimensions. In addition, excitons in InGaAs QRs have been studied within the effective-mass approximation [14], and a strong red-shift of transition peaks in the optical susceptibility was found.

Although most QR models assume an axially symmetric shape, the study of more realistic situations has addressed some attention. In particular, Magarill *et al* [15] have studied PCs in elliptical QRs. These authors have shown that the PC is a periodic function of the magnetic field intensity in elliptical rings, but the current amplitude is reduced as the eccentricity of the ellipse increases. In this paper, we present a theoretical study of electronic states in QRs limited by cylindrical surfaces, and analyse the effects of in-plane electric fields. Such QRs may be concentric or eccentric, where the eccentricity is the distance between the axes of the cylindrical faces. In this sense, a micrograph view of the mask used for the fabrication of etched GaAs–(Ga, Al)As QRs, reported by Philipp *et al* [16], suggests that real QRs may present some degree of eccentricity[3]. Such a lack of symmetry would produce a measurable built-in dipole moment [17]. Therefore, we believe that a detailed investigation of the electronic spectrum of eccentric QRs should help the understanding of optical spectroscopic measurements in QRs.

[3] Actually, the eccentricity is not apparent in their samples, as the authors stressed in a private communication.

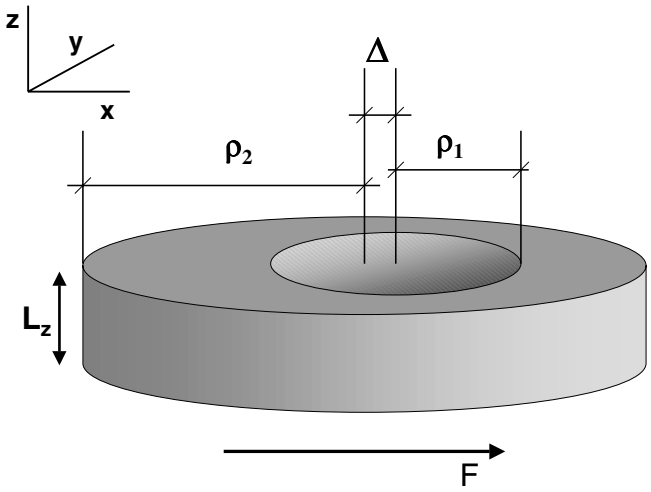

Figure 1. Schematic view of the eccentric quantum ring in the electric field F applied in the x-axis direction. $\rho_1(\rho_2)$ is the internal (external) radius, L_z is the height and Δ is the eccentricity.

2. Theoretical framework and results

To study the energies and wavefunctions of electrons in GaAs QRs we use a parabolic-band scheme within the effective-mass approximation. The confinement potential is chosen to be zero inside and infinite outside the QR. Hence, the wavefunction is zero in the latter region. The QR is a GaAs crystal limited by two cylinders of radii ρ_1 and ρ_2 ($\rho_2 > \rho_1$) with axes parallel to the z axis, and two parallel planes $z = \pm L_z/2$ (therefore, the xy plane bisects the QR). An schematic view of the quantum ring is shown in figure 1. The distance L_z between those planes defines the QR height, whereas the distance Δ between the axes is called the eccentricity (with $\Delta < L_\rho = \rho_2 - \rho_1$). When $\Delta = 0$ the ring is said to be concentric, otherwise it is eccentric. The internal and external cylindrical faces satisfy $(x - \Delta)^2 + y^2 = \rho_1^2$ and $x^2 + y^2 = \rho_2^2$, respectively. We also consider an electric field $\boldsymbol{F} = (F, 0, 0)$ applied in the x-axis direction. The Hamiltonian of a charge carrier with position vector $\boldsymbol{r}$ inside the GaAs QR is written as

$$\left(-\frac{\hbar^2}{2m^*}\nabla^2 + e\boldsymbol{F}\cdot\boldsymbol{r}\right)\Psi(\boldsymbol{r}) = \mathcal{E}\,\Psi(\boldsymbol{r}) \tag{1}$$

with $-e$ denoting the electron charge and m^* being the effective mass in GaAs (for conduction electrons we take $m_c^* = 0.067\,m_0$, where m_0 is the electron mass). As the z component of $\boldsymbol{F}$ is zero, the carrier dynamics may be separated in vertical (z axis) and in-plane (xy plane) motions, namely

$$\Psi\nu(\boldsymbol{r}) = Z_\nu(z)\,\psi\,(x, y)$$

where

$$Z_\nu(z) = \sqrt{\frac{2}{L_z}}\sin\left[\nu\pi\left(\frac{z}{L_z} + \frac{1}{2}\right)\right]$$

for $\nu = 1, 2, \ldots$, and $|z| \leqslant L_z/2$. The function $\psi\,(x, y)$ satisfies

$$\left[-\frac{\hbar^2}{2m^*}\nabla^2_{(x,y)} + eFx\right]\psi\,(x, y) = E\,\psi\,(x, y) \tag{2}$$

and $\mathcal{E}_v = v^2\pi^2\hbar^2/\left(2m^*L_z^2\right) + E$. In what follows, different cases for the in-plane motion are discussed.

2.1. Concentric ring with $F = 0$

In this case, the system has axial symmetry and we conveniently use polar coordinates (ρ, ϕ) to solve equation (2), with $\rho \geqslant 0$ and $-\pi < \phi \leqslant \pi$. However, we do not choose the states as eigenfunctions of the angular momentum projection in the z axis. Instead, states with defined parity in ϕ (or y, equivalently) are chosen. With this, the solutions may be written as

$$\psi^{(0)}_{m,l,\alpha}(\rho, \phi) = \frac{1}{\sqrt{\pi(1+\delta_l)}} R_{m,l}(\rho)\cos(l\phi - \alpha\pi/2) \tag{3}$$

with $\alpha = 0$ (even states) or $\alpha = 1$ (odd states), and $l \geqslant \alpha$ being an integer. Also, $\delta_l = 1$ ($\delta_l = 0$) if $l = 0$ ($l \neq 0$). The radial part is

$$R_{m,l}(\rho) = A_{m,l}J_l(\beta_{m,l}\rho) + B_{m,l}Y_l(\beta_{m,l}\rho) \tag{4}$$

where J_l and Y_l are the ordinary l-order Bessel functions and $\beta_{m,l}$ is the mth solution of

$$J_l(\beta\rho_1)Y_l(\beta\rho_2) = J_l(\beta\rho_2)Y_l(\beta\rho_1) \tag{5}$$

for $\beta > 0$, with $m \geqslant 1$. To guarantee orthonormalization, the coefficients $A_{m,l}$ and $B_{m,l}$ are chosen as

$$B_{m,l} = -A_{m,l}\frac{J_l(\beta_{m,l}\rho_1)}{Y_l(\beta_{m,l}\rho_1)} \tag{6}$$

with

$$A_{m,l} = (\beta_{m,l}\pi)\sqrt{\frac{2}{Y_l^2(\beta_{m,l}\rho_2)} - \frac{2}{Y_l^2(\beta_{m,l}\rho_1)}}. \tag{7}$$

Also, the energies are given by $E^{(0)}_{m,l} = \hbar^2\beta^2_{m,l}/(2m^*)$.

The wavefunction in equation (3) has rotation symmetry of order l for $l \geqslant 1$, and revolution symmetry for $l = 0$ (see figure 2(a1)), but has no symmetry in the radial direction. However, if the radial width $L_\rho = \rho_2 - \rho_1$ satisfies $L_\rho \ll \rho_1$ then the low-energy states exhibit approximate symmetry about the geometrical mean radius $\rho_g = (\rho_1 + \rho_2)/2$. In particular, the ground-state probability distribution $\rho\,|R_{1,0}(\rho)|^2$ reaches its maximum at points with radius $\rho = \rho^*_{1,0}$, and $\rho^*_{1,0} \to \rho_g$ monotonically as $\rho_2 \to \rho_1$. This behaviour is apparent in figure 3(a), where the rate $\rho^*_{1,0}/\rho_g$ is shown (broken curve) as a function of ρ_2/ρ_1.

The average value $\langle\rho/\rho_g\rangle_{m,0} = \langle R_{m,0}(\rho)|\rho/\rho_g|R_{m,0}(\rho)\rangle$ of ρ/ρ_g for the $R_{m,0}$ mode with $m = 1$, which is also displayed (full curve) in figure 3(a), shows a similar behaviour. It is important to stress that both $\rho^*_{1,0}$ and $\langle\rho\rangle_{1,0}$ equal ρ_g within a relative error of 2% for $\rho_2/\rho_1 < 10$. The latter relation is satisfied by most fabricated or grown QRs. Also, $\langle\rho\rangle_{m,0} \simeq \rho_g$ for $m = 2, \ldots, 12$ within a relative error of 0.2% for $\rho_2/\rho_1 < 10$, as shown in figure 3(b). This suggests that useful information on the electron states in such QRs may be obtained by considering separate radial and angular motions, even in the presence of an in-plane electric field. Namely, in such an approximation the radial motion is described by $R_{m,0}(\rho)$ with $m = 1, 2, \ldots$, whereas the angular motion is that of an electron in a purely one-dimensional QR with radius ρ_g subjected to the in-plane electric field. The results of this approximation are presented below.

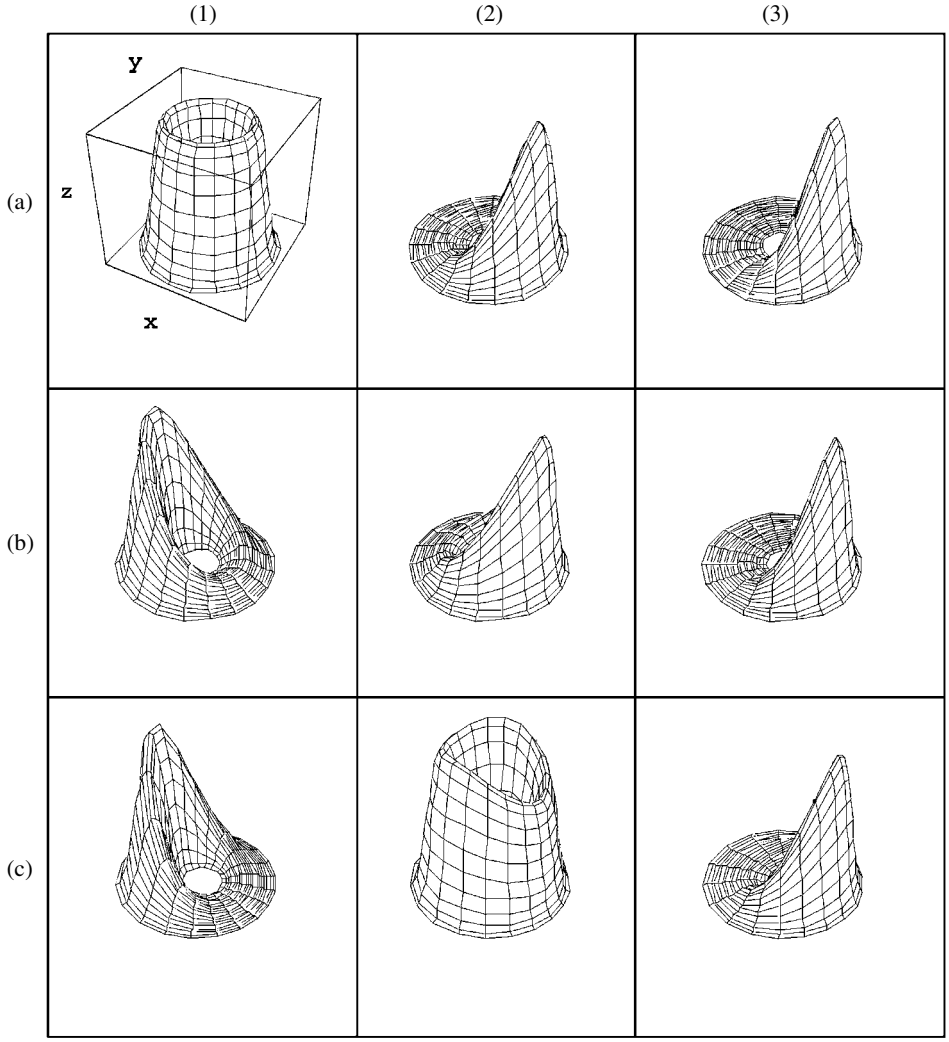

Figure 2. In-plane probability distribution for the ground state of an electron in GaAs QRs with $\rho_1 = 50$ Å and $\rho_2 = 200$ Å. Columns 1, 2 and 3 correspond to $F = 0$, -5 and -10 kV cm^{-1}, whereas rows (a)–(c) are for $\Delta = 0$, 10 and 20 Å, respectively.

2.2. Concentric ring with $F \neq 0$

In this case the electron energies and states for F and $-F$ coincide due to the QR symmetry, except for the mirror reflection $x \to -x$ in the wavefunctions. As the Hamiltonian is invariant under transformation $y \to -y$, its eigenfunctions may be chosen as

$$\psi_\alpha(\rho, \phi) = \sum_{l=\alpha}^{\infty} \sum_{m=1}^{\infty} c_{m,l}^{(\alpha)} \, \psi_{m,l,\alpha}^{(0)}(\rho, \phi) \tag{8}$$

for even ($\alpha = 0$) or odd ($\alpha = 1$) states. Substituting the latter expression in equation (2), one gets the eigensystem

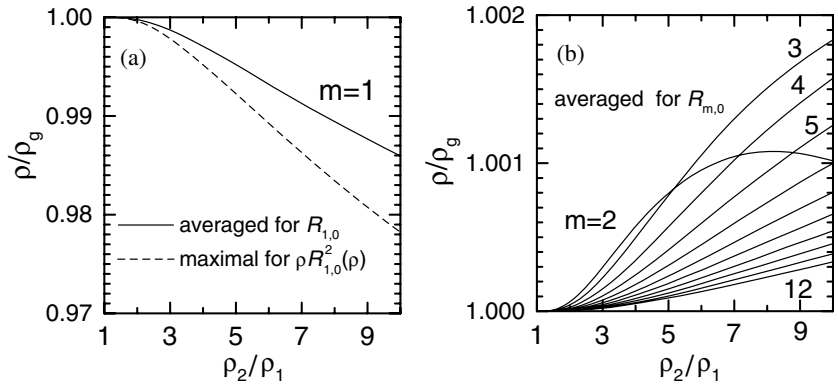

Figure 3. The averaged radius $\langle\rho\rangle_{m,0}$ (full curves) with (a) $m = 1$ and (b) $m = 2, \ldots, 12$ in units of the geometrical mean radius ρ_g as a function of the rate ρ_2/ρ_1, for a GaAs QR. The rate between the maximal radius $\rho^*_{1,0}$ for the ground-state probability distribution and ρ_g is also shown as a broken curve in (a).

$$\sum_{l'=\alpha}^{\infty}\sum_{m'=1}^{\infty}\left(E^{(0)}_{m,l}\,\delta_{l'-l}\,\delta_{m'-m} + eF\,M^{(\alpha)}_{m,l,m',l'}\right)c^{(\alpha)}_{m',l'} = E_\alpha\,c^{(\alpha)}_{m,l} \tag{9}$$

where $M^{(\alpha)}_{m',l',m,l} = M^{(\alpha)}_{m,l,m',l'}$ and

$$M^{(\alpha)}_{m,l,m',l'} = \frac{\delta_{l'-l-1}\sqrt{1+\delta_l}}{\left(\beta^2_{m,l}-\beta^2_{m',l+1}\right)^2}\left[\rho\frac{\mathrm{d}R_{m,l}(\rho)}{\mathrm{d}\rho}\,\frac{\mathrm{d}R_{m',l+1}(\rho)}{\mathrm{d}\rho}\right]^{\rho=\rho_2}_{\rho=\rho_1} \tag{10}$$

for $l' \geqslant l$. The energies $E_{\alpha,n}$ and coefficients $c^{(\alpha,n)}_{m,l}$ for $n \geqslant 1$ are obtained from equation (10) by diagonalization techniques, and therefore the in-plane wavefunctions are denoted by $\psi_{\alpha,n}(\rho,\phi)$, following equation (8).

The polarization of the ground state due to applied electric fields is apparent in figures 2(a2) and (a3) for $F = -5$ and -10 kV cm^{-1}, respectively. Note that $F < 0$ means lower electric potential to the left, and consequently electrons are pushed to the right. The dependence of the energy spectrum $E_{\alpha,n}$ for the in-plane motion with the electric field intensity F is displayed in figure 4, for $\rho_1 = 50$ Å and $\rho_2 = 200$ Å. In the calculations a set of $(13-\alpha)\times 12$ terms in equation (8) was considered, corresponding to $l = \alpha, \ldots, 12$ and $m = 1, \ldots, 12$. The complicated structure of the spectra is better understood if the separation of variables is considered. As mentioned above, the radial motion is described by $R_{m,0}(\rho)$ with $m = 1, 2, \ldots$, whereas the angular motion is that of an electron in a purely one-dimensional (1D) QR with radius ρ_g subjected to the in-plane electric field. Hence, the in-plane energy spectrum is obtained by shifts in $E^{(0)}_{m,0}$ of the spectrum for the 1D ring[4]. The results of this approximation are shown in figure 4, where broken, dotted and chain curves correspond to $m = 1$, 2, and 3, respectively. One may clearly note that low-energy levels and anticrossings between them are well explained with the separation of variables. An important result is that the variation of lower levels is mainly due to the ring shape and not to the finite width L_ρ.

The polarization or induced dipole moment for electron states corresponding to the five lower levels is shown in figure 5 for (a) even and (b) odd levels. By symmetry, the polarization occurs in the x-axis direction, and its value is calculated as

[4] The details of this spectrum, which involves the Mathieu equation, will be presented elsewhere.

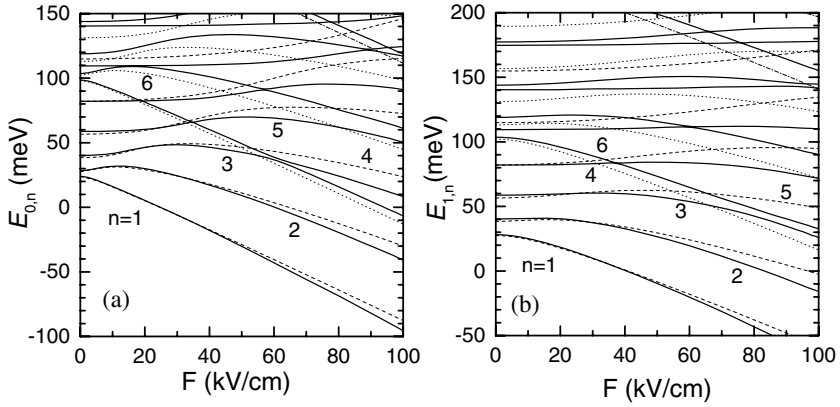

Figure 4. Electron energy levels $E_{\alpha,n}$ (full curves) for (a) even and (b) odd states as functions of the electric field intensity F for a GaAs QR with $\rho_1 = 50$ Å and $\rho_2 = 200$ Å. Broken, dotted and chain curves correspond to the $m = 1$, 2 and 3 energy-level aproximations, respectively, based on the separation of variables.

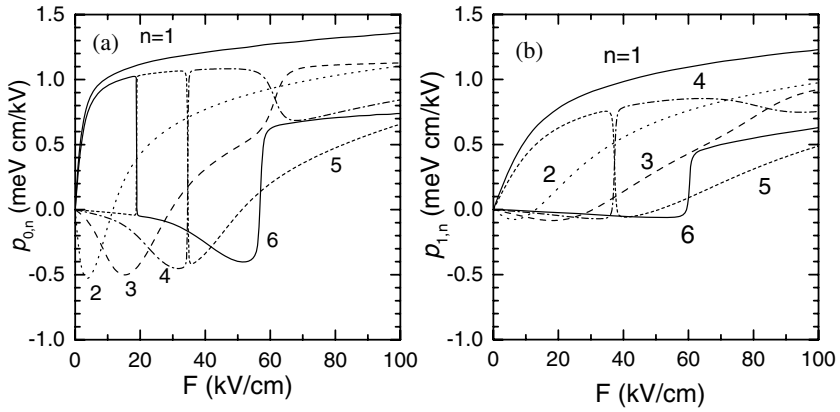

Figure 5. Polarization $p_{\alpha,n}$ of (a) even and (b) odd states as a function of the electric field intensity F for a GaAs QR with $\rho_1 = 50$ Å and $\rho_2 = 200$ Å.

$$p_{\alpha,n} = -e \int_{-\pi}^{\pi} \int_{\rho_1}^{\rho_2} |\psi_{\alpha,n}(\rho, \phi)|^2 \rho^2 \cos(\phi)\ \mathrm{d}\rho\, \mathrm{d}\phi \tag{11a}$$

$$= -2e \sum_{l=\alpha}^{\infty} \sum_{m=1}^{\infty} \sum_{m'=1}^{\infty} c_{m,l}^{(\alpha,n)}\ M_{m,l,m',l+1}^{(\alpha)} c_{m',l+1}^{(\alpha,n)}. \tag{11b}$$

In figure 5 it is clear that $n = 1$ states show increasing polarization with the field intensity, as would be expected for a charged cloud without nodes under applied electric fields. States with $n > 1$ show a complex behaviour both in energy and polarization. Indeed, energy and polarization satisfy the relation

$$p_{\alpha,n} = -\frac{\partial E_{\alpha,n}}{\partial F} \tag{12}$$

which allows a better understanding of figure 5 from figure 4. As may be noted, odd states show smaller polarization than even ones. This is due to the existence of wavefunction nodes at

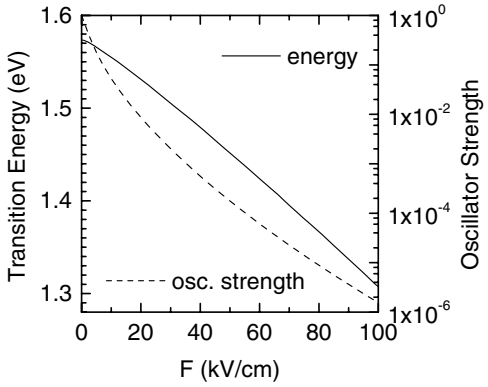

Figure 6. Interband ground-to-ground level transition energy (full curve) and oscillator strength (broken curve) as functions of F for a QR with $\rho_1 = 50$ Å, $L_z = L_\rho = 150$ Å.

the x axis for odd states. This reduces the probability values at the left and right regions in the ring, i.e. reduces the effective size of the QR in the field direction. The negative polarization of states with $n > 1$ (see figure 4), which is called anomalous, is explained by the orthogonality correlation (coupling) between wavefunctions of different levels [11].

A strong dependence of the electron ground level $E_{0,1}$ on F is apparent in figure 4, suggesting a possible experimental control of the ground-state energy in QRs. This may be performed by measuring the interband absorption spectrum [16]. As a first approximation for the peak positions, one may determine the free electron–hole recombination energy by using a simple parabolic band for the holes in GaAs. In doing this, we substitute $e \to -e$ and $m^* \to m_h^*$ in equation (2), where $m_h^* = 0.34\, m_0$ is the heavy-hole effective mass for GaAs. We determine the photon energy of the first peak from the energies $E_{0,1}^{(c)}$ and $E_{0,1}^{(h)}$ of the conduction and hole ground levels, respectively. The recombination energy $E_g + E_{0,1}^{(c)} + E_{0,1}^{(h)} + \pi^2\hbar^2\left(m_c^* + m_h^*\right) / \left(2m_c^* m_h^* L_z^2\right)$ is plotted in figure 6 as a function of F, where $E_g = 1.52$ eV is the GaAs energy gap. The oscillator strength, which may be calculated as

$$T_{\alpha,n_h,n_c} = \int_{-\pi}^{\pi}\int_{\rho_1}^{\rho_2} \psi_{\alpha,n_h}(\rho,\phi)\psi_{\alpha,n_c}(\rho,\phi)\rho\,\mathrm{d}\rho\,\mathrm{d}\phi \tag{13a}$$

$$= \sum_{l=\alpha}^{\infty}\sum_{m=1}^{\infty} c_{m,l}^{(\alpha,n_h)} c_{m,l}^{(\alpha,n_c)} \tag{13b}$$

is also shown in figure 6 for $\alpha = 0$ and $n_h = n_c = 1$, corresponding to the ground-to-ground transition. Note that the oscillator strength strongly decreases as F increases, due to the opposite and increasing polarizations of electron and holes. In calculations we consider a QR with $\rho_1 = 50$ Å and $L_z = L_\rho = 150$ Å. Of course, a better theoretical description would include excitonic effects and mixing of light and heavy hole states. In this sense, it should be stressed that the values of oscillator strength are underestimated in the above prediction. Actually, the Coulomb attraction between electron and hole should enhance the oscillator strength when the exciton is considered. However, the present approach for interband transitions illustrates important effects of in-plane fields for optical investigations concerning QR structures.

2.3. Eccentric ring with $F = 0$

For eccentric rings ($\Delta \neq 0$), one has to solve equation (2) within the ring $\mathcal{R}$ between the circumferences $(x-\Delta)^2 + y^2 = \rho_1^2$ and $x^2 + y^2 = \rho_2^2$, where solutions $\psi(x, y)$ must vanish at the boundary of $\mathcal{R}$. Alternatively, we make a transformation of coordinates, such that circular boundaries become concentric. This is performed by introducing the complex variable $\omega = x + \mathrm{i}y$, and a conformal transformation $\omega' = x' + \mathrm{i}y' = f(\omega)$ which maps $\mathcal{R}$ onto the ring $\mathcal{R}'$, limited by $|\omega'| = \rho_1'$ and $|\omega'| = \rho_2$. Such a transformation is called bilinear and is written as [18]

$$\omega' = \frac{\omega - x_0}{1 - x_0\omega/\rho_2^2} \tag{14}$$

where

$$x_0 = \frac{1 + L_1L_2 - \sqrt{(1-L_1^2)(1-L_2^2)}}{2\Delta/\rho_2^2} \tag{15}$$

with L_1 and L_2 given by $(\Delta-\rho_1)/\rho_2$ and $(\Delta+\rho_1)/\rho_2$, respectively. Note that $\mathcal{R}'$ is a concentric ring with internal radius given by

$$\rho_1' = \frac{1 - L_1L_2 - \sqrt{(1-L_1^2)(1-L_2^2)}}{2\rho_1/\rho_2^2}. \tag{16}$$

At the same time, equation (2) for $F = 0$ is transformed to

$$-\frac{\hbar^2}{2m^*J(x', y')}\nabla^2_{(x',y')}\tilde{\psi}(x', y') = E\,\tilde{\psi}(x', y') \tag{17}$$

where $\tilde{\psi}(x', y') = \psi(x, y)$ must vanish at the boundary of $\mathcal{R}'$, and $J(x', y') = g(x', y')^{-2}$ with

$$g(x', y') = \frac{\left(1 + x_0x'/\rho_2^2\right)^2 + \left(x_0y'/\rho_2^2\right)^2}{(1 - x_0^2/\rho_2^2)} \tag{18}$$

is the Jacobian of the coordinate transformation $(x', y') \to (x, y)$. The Hamiltonian in equation (17) is rather complicated, but it is invariant under transformation $y' \to -y'$. Hence, using polar coordinates (ρ', ϕ') the eigenfunctions may be chosen as

$$\tilde{\psi}_\alpha(\rho', \phi') = g(x', y')\sum_{l=\alpha}^{\infty}\sum_{m=1}^{\infty} c_{m,l}^{(\alpha)}\tilde{\psi}_{m,l,\alpha}^{(0)}(\rho', \phi') \tag{19}$$

for even ($\alpha = 0$) or odd ($\alpha = 1$) states, where the functions $\tilde{\psi}_{m,l,\alpha}^{(0)}(\rho', \phi')$ satisfy equation (17) if $J(x', y')$ and E are substituted by 1 and $E_{m,l}^{(0)}$, respectively. The resulting equation describes the in-plane motion of an electron in the concentric ring $\mathcal{R}'$, and we obtain its solutions following section 3.1. After solving the eigensystem

$$\sum_{l'=\alpha}^{\infty}\sum_{m'=1}^{\infty} N_{m,l,m',l'}^{(\alpha)}\, c_{m',l'}^{(\alpha)} = E_\alpha c_{m,l}^{(\alpha)} \tag{20}$$

with

$$N_{m,l,m',l'}^{(\alpha)} = \frac{E_{m,l}^{(0)} + E_{m',l'}^{(0)}}{2}\int_{-\pi}^{\pi}\int_{\rho_1'}^{\rho_2}\frac{\tilde{\psi}_{m,l,\alpha}^{(0)}(\rho', \phi')\,\tilde{\psi}_{m',l',\alpha}^{(0)}(\rho', \phi')}{J(x', y')}\rho'\,\mathrm{d}\rho'\,\mathrm{d}\phi' \tag{21}$$

$$+\frac{6\hbar^2x_0^2}{m^*\rho_2^4(1 - x_0^2/\rho_2^2)}\int_{-\pi}^{\pi}\int_{\rho_1'}^{\rho_2} g(x', y')\;\tilde{\psi}_{m,l,\alpha}^{(0)}(\rho', \phi')$$
$$\times\tilde{\psi}_{m',l',\alpha}^{(0)}(\rho', \phi')\;\rho'\,\mathrm{d}\rho'\,\mathrm{d}\phi' \tag{22}$$

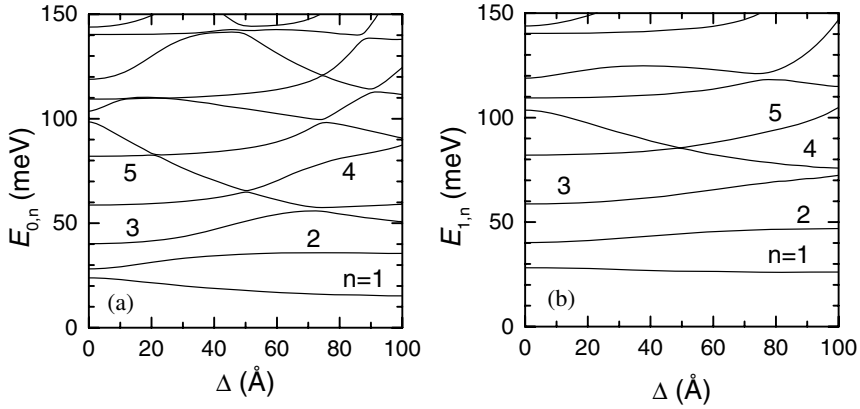

Figure 7. The electron energy levels $E_{\alpha,n}$ for (a) even and (b) odd states as functions of the eccentricity Δ for a QR with $\rho_1 = 50$ Å and $\rho_2 = 200$ Å.

the energies $E_{\alpha,n}$ and coefficients $c_{m,l}^{(\alpha,n)}$, for $n = 1, 2, \ldots$, are obtained. The wavefunctions $\psi_{\alpha,n}(x, y) = \tilde{\psi}_{\alpha,n}(\rho', \phi')$ form an orthonormal set if the eigenvectors $c^{(\alpha,n)}$ are normalized.

The electron energy levels $E_{\alpha,n}$ are displayed in figure 7 as functions of the eccentricity Δ, for a QR with $\rho_1 = 50$ Å and $\rho_2 = 200$ Å. In the calculations we considered $(17-\alpha) \times 12$ terms in equation (8), corresponding to $l = \alpha, \ldots, 16$ and $m = 1, \ldots, 12$. One may notice that the dependence of lower levels (odd and even states) on the eccentricity value is relatively weak, even for $\Delta \sim \frac{2}{3}L_\rho$. In particular, for small Δ (less than 10 Å) the levels do not change more than 1.3 meV with eccentricity. One may conclude that eccentricities in this range, which covers most undesired defects in high-quality growth or fabrication, would produce very small shifts in the peak positions of optical spectra involving such levels. In contrast, the wavefunctions are far more sensitive to eccentricity and a strong polarization of electron states occurs even for small values of Δ (see figures 2(b1) and (c1)). Hence, oscillator strengths in optical spectra should appreciably depend on eccentricity, as occurs in the presence of in-plane electric fields (see figure 6).

2.4. Eccentric ring with $F \neq 0$

The interplay between electric field and eccentricity effects on the electronic energy spectra in QRs is also investigated. In this case the electron states for F and $-F$ differ due to eccentricity. To consider the applied electric field, the term

$$\frac{eF\rho_2^2}{x_0}\left[1 - \frac{\left(1 + x_0 x'/\rho_2^2\right)}{g\,(x', y')}\right] \tag{23}$$

is included in the Hamiltonian of equation (17), and the resulting equation is solved in analogy with section 2.3. The in-plane probability distributions for the ground state in a GaAs QR with $\rho_1 = 50$ Å and $\rho_2 = 200$ Å are displayed in figure 2. Columns 1, 2 and 3 correspond to $F = 0$, -5 and -10 kV cm^{-1}, whereas rows (a)–(c) are for $\Delta = 0$, 10 and 20 Å, respectively. Negative values of F are taken in order to produce a polarization opposed to that due to eccentricity. As already discussed, the revolution symmetry in figure 2(a1) for $F = 0$ kV cm^{-1} and $\Delta = 0$ Å is clearly broken by electric field and eccentricity effects. One may expect the polarizations induced by those effects to compensate, somehow, for appropriate

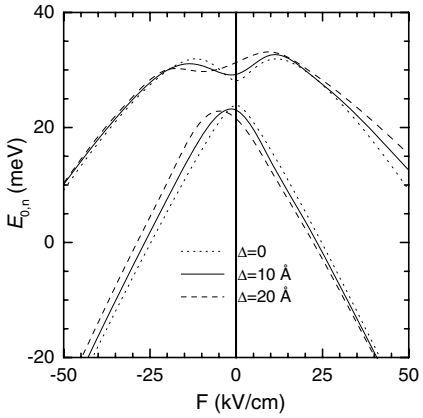

Figure 8. The lower two in-plane energy levels for even states as functions of the electric field intensity F for GaAs QRs with $\rho_1 = 50$ Å, $\rho_2 = 200$ Å, and different values of the eccentricity Δ. Dotted, full and broken curves are for $\Delta = 0$, 10 and 20 Å, respectively.

values of Δ and F. Such a compensation is apparent in figure 2(c2) for $F = -5$ kV cm^{-1} and $\Delta = 20$ Å. Weaker compensations are shown in figures 2(b2), (b3) and (c3).

In figure 8, the two lower energy levels corresponding to even states (in ϕ) are plotted as functions of the electric field intensity F, for GaAs QRs with $\rho_1 = 50$ Å, $\rho_2 = 200$ Å and different values of the eccentricity $\Delta = 0$, 10 and 20 Å. As may be noted, the slope on energy levels at $F = 0$ is zero for concentric QRs, whereas it is not for eccentric ones. Following equation (12), it means that one-electron eccentric rings have a built-in dipole moment. As hole states polarize in the opposite direction, states of electron and holes in an eccentric QR are expected to be polarized too. Furthermore, the compensation between electric field and eccentricity induced polarizations should occur at stationary values of F, for which the energy slope vanishes. This is the case for the lower broken curve ($\Delta = 20$ Å) in figure 8 at $F \simeq -5$ kV cm^{-1}, in agreement with figure 2(c2).

3. Conclusions

We have presented a detailed analysis of the electronic properties of semiconductor QRs, giving emphasis to electric field and eccentricity effects on the spectra of GaAs QRs. For simplicity, we have chosen the infinite potential model. In this case, the energy spectrum remains discrete when applied electric fields are considered. For finite barriers, quasi-stationary states of a continuous spectrum should be considered. When eccentricity is taken into account, a conformal mapping allows a relatively simple solution of the Schrödinger equation for infinite barriers. Instead, further mathematical discussions are needed for finite barriers, since the bilinear transformation (see equation (14)) is not analytic outside the ring. For a parabolic confinement model with strong in-plane electric field, the low-energy levels should manifest a quadratic decrease with field intensity. This behaviour contrasts with the linear dependence of the ground level at high fields for infinite barrier QRs. Instead, for low fields both models are expected to give similar qualitative behaviours. We believe, however, that our results are meaningful for experimental QRs if low-energy levels and moderate electric fields are considered.

The electronic energy spectrum is shown to strongly depend on the intensity of the applied electric field exhibiting similar qualitative features as the energy spectrum of electrons

in a quantum well previously reported [19]. This makes the interband optical absorption measurement an appropriate technique to monitor the energy levels in QRs under in-plane electric fields. In this sense, the induced polarization affects the interband oscillator strength, and for the ground-to-ground transition its value strongly decreases with the field intensity. Unexpectedly, this is in contrast with the results of Llorens *et al* [11] for a QR, even if one takes into account the difference between the QR parameters in calculations.

On the other hand, the eccentricity is included in the theoretical framework as a tentative parameter to model the natural defects on the experimental realization of QRs. While lower energy levels are weakly dependent on the eccentricity value, the corresponding wavefunctions are quite sensitive to the lack of symmetry. Hence eccentricity should produce a built-in dipole moment and affect the oscillator strength in optical absorption. Also, the competition between applied electric fields and eccentricity has been analysed, and their polarization effects were found to compensate for appropriate values of them. This reinforces the usefulness of applied fields in tailoring the properties of different materials and structures.

Finally, taking into account the increasing number of experimental techniques developed to generate self-assembled quantum ring and dot arrays, we believe that a better understanding of the physical properties of QRs should help the development of optoelectronic devices based on such nanostructures.

Acknowledgments

We would like to thank M Pacheco and Z Barticevic for useful suggestions and the Brazilian agencies CNPq, CAPES and FAPESP for partial financial support. ABA is grateful to colleagues E M Rosa and V Locci for useful discussions.

References

[1] Mendez E E, Bastard G, Chang L L, Esaki L, Morkoc H and Fischer R 1982 *Phys. Rev.* B **26** 7101
[2] Casado E and Trallero-Giner C 1996 *Phys. Status Solidi* b **196** 335
[3] Susa N 1996 *IEEE J. Quantum Electron.* **32** 1760
[4] Peyghambarian N, Koch S W and Mysyrowicz A 1993 *Introduction to Semiconductor Optics* (Englewood Cliffs, NJ: Prentice-Hall)
Haug H and Koch S W 1994 *Quantum Theory of the Optical and Electronic Properties of Semiconductors* (Singapore: World Scientific)
[5] Warburton R J, Schaflein C, Haft D, Bickel F, Lorke A, Karrai K, Garcia J M, Schoenfeld W and Petroff P M 2000 *Nature* **405** 926
[6] Lorke A, Luyken R J, Govorov A O, Kotthaus JP, Garcia J M and Petroff P M 2000 *Phys. Rev. Lett.* **84** 2223
Lorke A and Luyken R J 1998 *Physica* B **256** 424
[7] Mailly D, Chapelier C and Benoit A 1993 *Phys. Rev. Lett.* **70** 2020
[8] Lin M F and Chui D S 1998 *Phys. Rev.* B **57** 6731
[9] Petterson H, Warburton, R J, Lorke A, Karrai K, Kotthaus J P, Garcia J M and Petroff P M 2000 *Physica* E **6** 511
[10] Barticevic Z, Pacheco M and Latgé A 2000 *Phys. Rev.* B **62** 6963
[11] Llorens J M, Trallero-Giner C, Garcia-Cristóbal A and Cantarero A 2001 *Phys. Rev.* B **64** 035 309
[12] Bruno-Alfonso A and Latgé A 2000 *Phys. Rev.* B **61** 13 885
[13] Song J and Ulloa S E 2001 *Phys. Rev.* B **63** 125 302
[14] Hu H, Li D J, Zhu J L and Xiong J J 2000 *J. Phys.: Condens. Matter* **12** 9145
[15] Magarill L I, Romanov D A and Chaplik A V 1996 *JETP* **83** 1063
[16] Philipp G E, Mejia Galeana J A, Cassou C, Wang P D, Guash C, Vögele B, Holland M C and Sotomayor Torres C M 1995 *Diagn. Techniques Semicond. Mater. Process. II* **409** 350
[17] Barker J A and O'Reilly E P 2000 *Phys. Rev.* B **61** 13 840
[18] Kreyszig E (ed) 1993 *Advanced Engineering Mathematics* 7th edn (New York: Wiley)
[19] Enderlein R, Holz T and Gondar J L 1989 *Phys. Status Solidi* b **156** 259